SUPPLEMENTAL INFORMATION

Supplemental Figure 1, related to Figure 1. The impact of GDP on respiration in permeabolized human adipose tissue. We developed a protocol for determining GDP sensitive mitochondrial respiration in intact human adipose tissue as shown in **Figure 1**. Adipose tissue sampled from below the platysma muscle (sBAT), above the platysma muscle (neck sWAT) and the forearm (arm sWAT) from the same individual were suspended in an air-tight respiration chamber in 2 mls of respiration buffer and permeabilized by the addition of 2µM digitonin. (**a**) Determination of an optimal GDP titration to assay UCP1 function in permeabilized human sBAT. Substrates (1.5 mM octanoyl-l-carnitine, 5 mM pyruvate, 2 mM malate, 10 mM glutamate and 10 mM succinate) were titrated into the oxygraph chamber to support leak respiration. Thereafter, GDP was sequentially titrated into the chamber at 2 to 4 mM increments. GDP titration inhibits sBAT mitochondrial respiration in a concentration dependent manner up to approximately 10-15 mM concentrations. Thereafter, further titration of GDP had no effect on respiration, suggesting a concentration of 15 to 20 mM GDP is sufficient to fully inhibit UCP1 in human sBAT. (**b**) GDP titration has little effect on respiration in neck sWAT. (**c**) Similarly, GDP titration had little impact on forearm sWAT mitochondrial respiration. It should be noted that respiratory fluxes were 80 to 130-fold lower in sWAT samples compare to sBAT, making the determination of GDP sensitivity (if any) in sWAT a challenge. Of note, following inhibition of respiration by GDP in sBAT (panel **a**), titration of the ionophore CCCP did not increase respiration to rates comparable to those prior to GDP titration, whereas titration of CCCP increased

respiration in both neck (panel **b**) and arm (panel **c**) sWAT to rates higher that those after titration of substrates. (**d**) Comparison of UCP1 dependent mitochondrial respiration in sWAT from the forearm, sWAT harvested from the neck (above the platysma muscle), and sBAT harvested below the platysma muscle.

Supplemental Figure 2, related to Figure 1. Mitochondrial coupling control in human and murine white and brown adipose tissue. (**a**) The leak control ratio for human sWAT and sBAT calculated from respiration data presented in Figure 1 by dividing state 2 by state 2_U respiration. (**b**) The leak control ratio for murine sWAT and sBAT calculated from respiration data presented in Figure 1 by dividing state 2 by state 2_U respiration. (**c**) The leak control ratio for human sWAT and sBAT calculated from respiration data presented in Figure 1 by dividing state 2_{GDP} respiration by state 2_U. (**d**) The leak control ratio for murine sWAT and sBAT calculated from respiration data presented in Figure 1 by dividing state 2_{GDP} respiration by state 2_U respiration. (**e**) The relative difference in UCP1 function (GDP sensitive respiration) in human sWAT and sBAT and murine iWAT and iBAT calculated from respiration data presents in Figure 1 showing similar differences in UCP1 function between WAT and BAT in humans and rodents.

Supplemental Figure 3, related to Figure 4. Regional anatomical differences in human adipose tissue mitochondrial respiratory capacity, coupling control, and flux control. As presented in **Figure 4**, adipose tissue sampled from above and below the platysma muscle has hugely different mitochondrial respiratory function. Here we

present further evidence of altered mitochondrial respiratory capacity and coupling control in these adipose tissue samples. (**a**) Mitochondrial respiratory capacity and coupling control in sWAT harvested from the forearm. (**b**) Mitochondrial respiratory capacity and coupling control in sWAT harvested from the left side of the neck above the platysma muscle. (**c**) Mitochondrial respiratory capacity and coupling control in sWAT harvested from the left side of the neck above the platysma muscle. (**d**) Mitochondrial respiratory capacity and coupling control in sBAT harvested from the left side of the neck below the platysma muscle. (**e**) Mitochondrial respiratory capacity and coupling control in sBAT harvested from the left side of the neck below the platysma muscle. In panels **a** – **e** mitochondrial respiratory capacity and coupling control were determined following the sequential titration of substrates (1.5 mM octanoyl-l-carnitine, 5 mM pyruvate, 2 mM malate and 10 mM glutamate), ADP (5 mM), succinate (10 mM), and oligomycin (5 µM). These data (**a-e**) highlight the large gradient in respiratory capacity of human WAT and BAT, and the complete lack of any coupling control in BAT, where ADP blocks respiration. (**f**) Mitochondrial respiratory capacity and flux control in sWAT harvested from the forearm. (**g**) Mitochondrial respiratory capacity and flux control in sWAT harvested from the right side of the neck above the platysma muscle. (**h**) Mitochondrial respiratory capacity and flux control in sWAT harvested from the right side of the neck above the platysma muscle. (**i**) Mitochondrial respiratory capacity and coupling control in sBAT harvested from the right side of the neck below the platysma muscle. (**j**) Mitochondrial respiratory capacity and coupling control in sBAT harvested from the right side of the neck below the platysma muscle. In panels **f** – **j** mitochondrial respiratory capacity and coupling control was determined following the sequential

titration of substrates (1.5 mM octanoyl-l-carnitine, 5 mM pyruvate, 2 mM malate and 10 mM glutamate), ADP (5 mM), succinate (10 mM), cytochrome C (10 µM), and CCCP (5 µM). These data (**f-j**) again highlight the significant gradient in oxidative capacity between human BAT and WAT, and the absence of flux control in human BAT mitochondria, where leak (state 2) respiration in almost uninhibited prior to ADP titration. Note that leak respiration prior to titration of substrates into the Oxygraph chamber is supported by endogenous substrates, likely FFAs.

Supplemental Figure 4, related to Figure 4. Mitochondrial enzyme activity and mitochondria specific respiratory capacity in human sBAT and sWAT. In **Figure 4** we presented data from one patient suggesting that greater mitochondria protien levels could largely (but not completely) explain the gradient in respiratory capacity seen between sBAT and sWAT. Here we show in a cohort of inidvidulas that Citrate synthase (CS) and Cytochrome C oxidase (COX) activity are significnatly higher in sBAT vs. sWAT, suggesting greater mitochondrial volume in sBAT. Further, while this difference in mitochodnrial protein partially explain greater respiratory capacity in sBAT, leak and in particular UCP-depedent leak respiration remain signifcantly greater in sBAT vs. sWAT when expressed per unit of mitochondrial enzyme activity. (**a**) CS activity in sWAT and sBAT samples from the same (n=5) individuals. (**b**) State 2 respiration normalized to CS activity in sWAT and sBAT samples from the same (n=5) individuals. (**c**) UCP1-dependent respiration normalized to CS activity in sWAT and sBAT samples from the same (n=5) individuals. (**d**) COX activity in sWAT and sBAT samples from the same (n=4) individuals. (**e**) State 2 respiration normalized to COX activity in sWAT and

sBAT samples from the same (n=4) individuals. (**f**) UCP1-dependent respiration normalized to COX activity in sWAT and sBAT samples from the same (n=4) individuals.

Supplemental Figure 5, related to Figure 1 and Figure 2. In **Figure 1** and **Figure 2** we present physiological, morpholical and genetic data from human and mouse BAT and WAT. Given the difficulty in sampling human sBAT, it can be difficult to perform comphrensive analysis of samples. Here we present physiological, morphological and genetic evidence of thermogenically functional supraclavicular brown adipose tissue in a human volunteer that had ~186 grams of BAT (determined by PET-CT). (**a**) Employing a novel PET-CT guided biopsy technique, sBAT was visualized prior to a per-cutaneous biopsy. (**b**) High resolution respirometry performed on fresh tissue samples revealed that sBAT of this individual had a respiratory capacity apporximately 100-fold greater than abdominal sWAT, and that the majority of this respiration can be inhibited by purine nucleotides. (**c**) Immunofluorescence demonstrates that in comparison to abdominal sWAT, human sBAT has an abundance of multilocular cells which are reactive to UCP1. Human sBAT also expresses high levels of thermogenic transcripts UCP1 and kcnk3 (**d** and **e**) and transcripts in volved in mitochondrial abunadnce and oxidative fucntion (**f** and **g**).

Supplemental Figure 1.

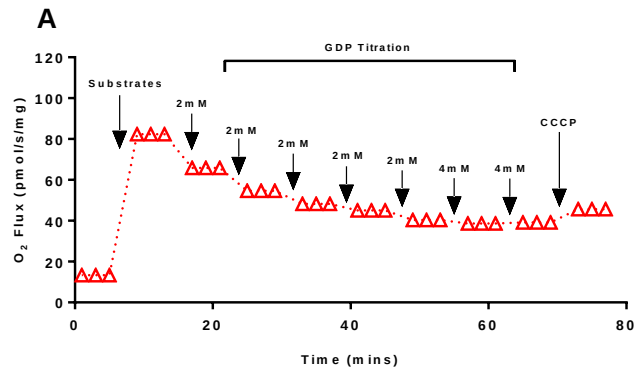

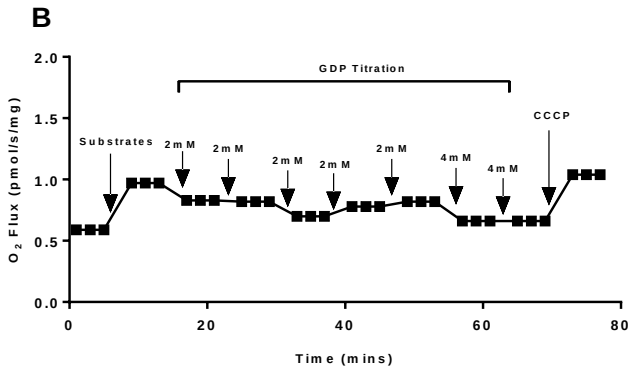

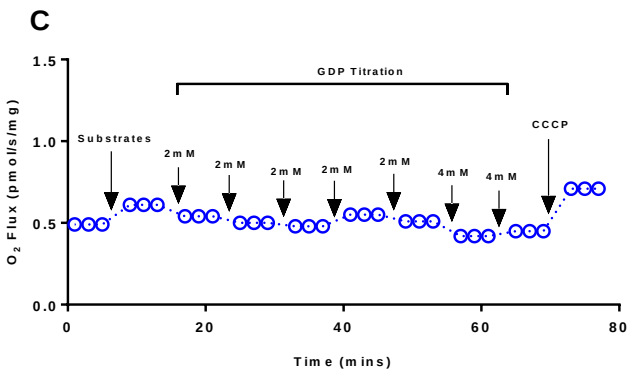

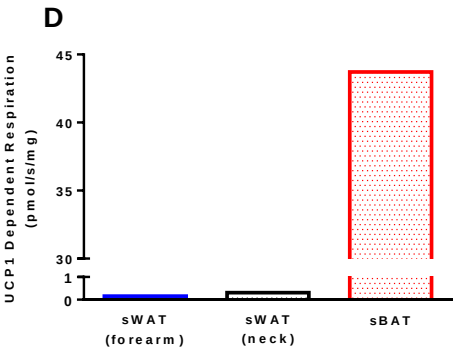

Supplemental Figure 2.

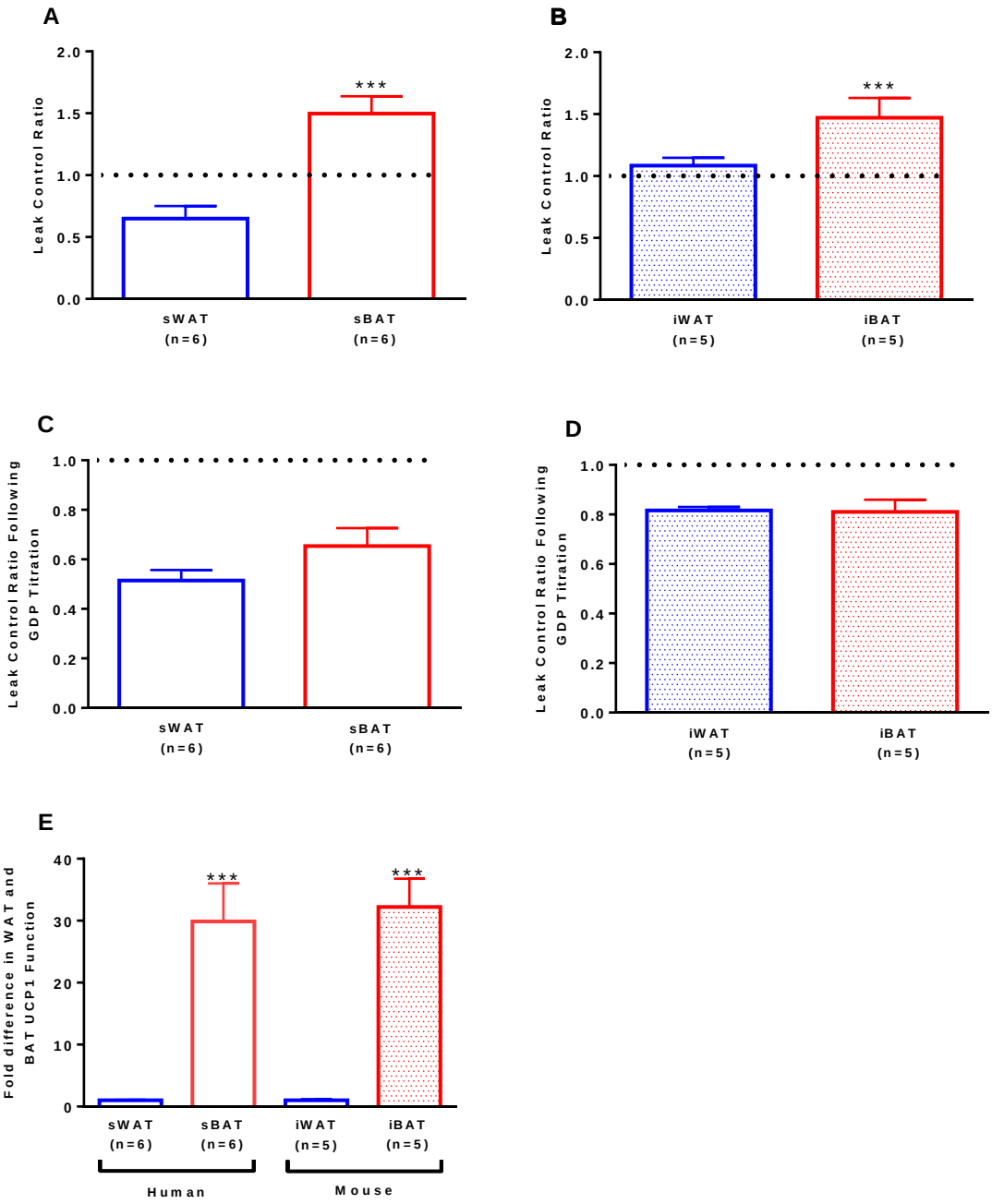

Supplemental Figure 3.

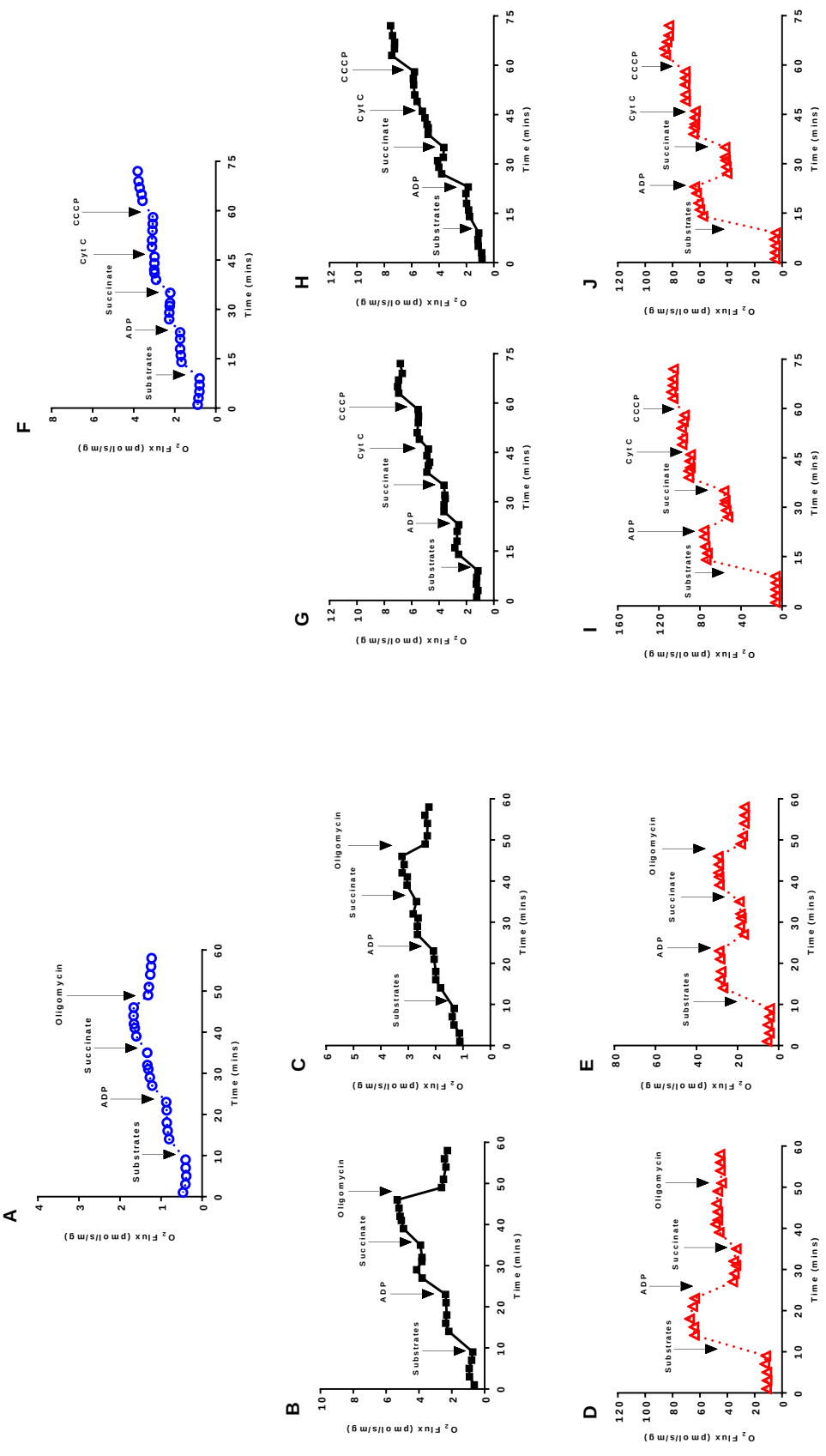

Supplemental Figure 4

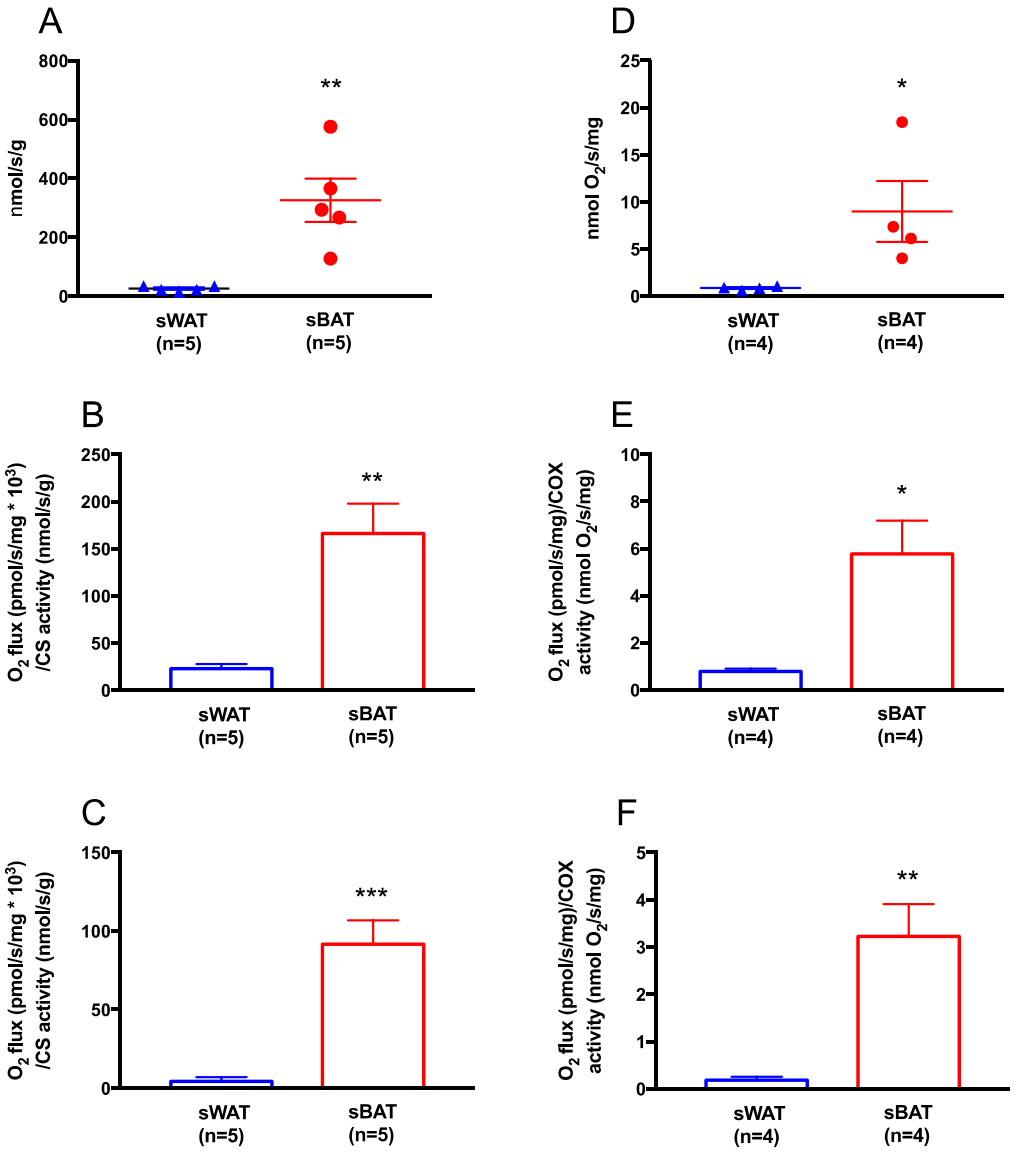

Supplemental Figure 5.

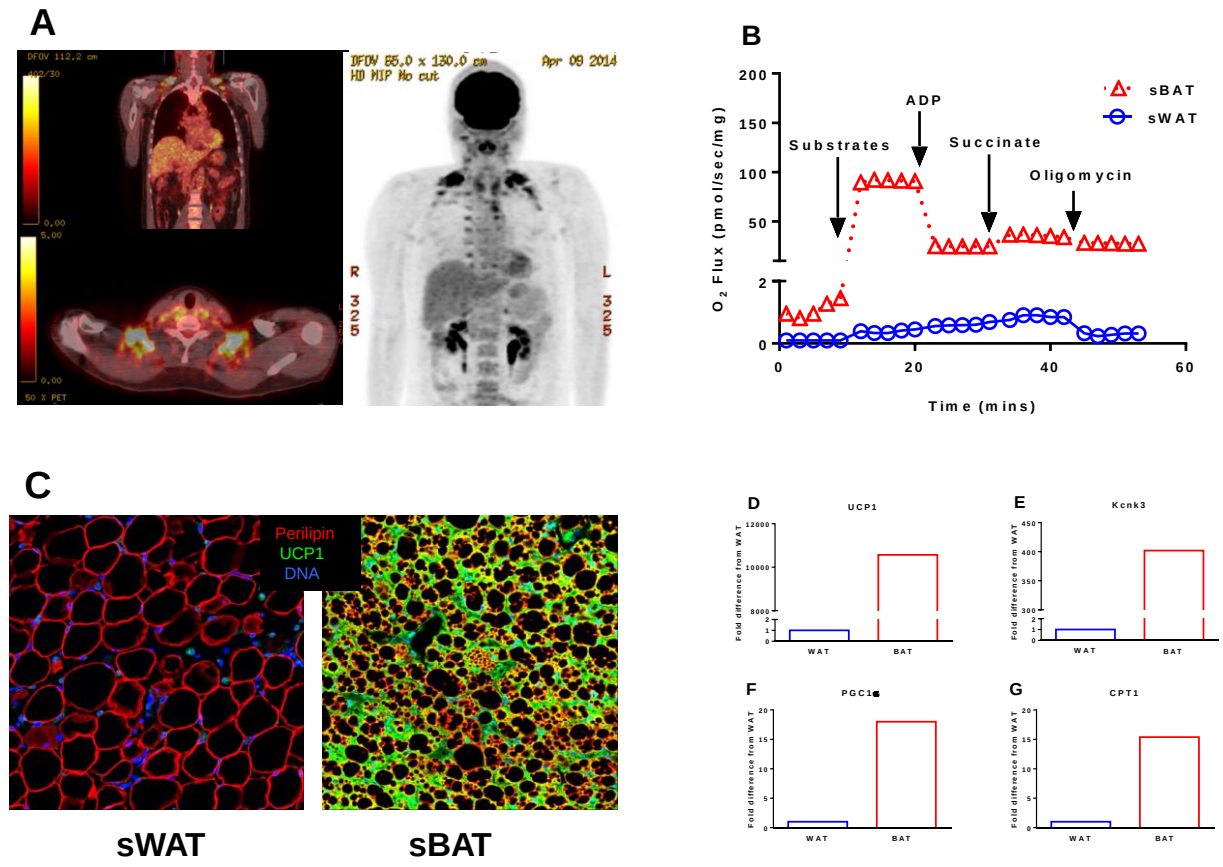

Experimental Procedures

Human Subjects.

All human research procedures were approved by the Institutional Review Board at the University of Texas Medical Branch. For studies involving radiological imaging of BAT and biopsy sampling of BAT and WAT,) healthy men were recruited and studied (PET-CT guided BAT Biopsies. These individuals were screened for health status, smoking, alcohol and drug histories, and current medication and dietary supplement use. Only healthy individuals who were not taking any medications for metabolic diseases were eligible to participate. In total, n=5 middle-aged men (43±14 years, mean±SD) weighing 93±16 kg (32% fat mass and 68% fat free mass) were recruited. These participants were metabolically healthy with a BMI of 28±5 kg/m^2.

In addition, one severely burned (39% of the total body surface area burned) pediatric (9 years old) patient who required burn scar release with local myofasciocutaneous flap reconstruction, was studied. During surgical reconstruction of burns involving the neck, sub-platysmal peri-jugular (carotid sheath) deep cervical adipose tissue was trimmed. This tissue was noted to be subtly darker in color than the subcutaneous adipose tissue sampled from above the platysma muscle. Subcutaneous adipose tissue was also collected from the forearm of this patient. Harvesting of sub-platysmal peri-jugular adipose tissue and subcutaneous adipose tissue above the platysma muscle was performed on both the left and right side of the neck.

Finally, skeletal muscle biopsies were obtained from six young (27±4 years, mean±SD) metabolically healthy men with a BMI of 28±3 (mean±SD) (see skeletal muscle sampling).

Cold-Exposure PET-CT guided BAT Biopsies

We have recently published a detailed description of a novel PET-CT guided percutaneous needle biopsy technique which allows the supraclavicular brown adipose (sBAT) depot of humans to be sampled (Chondronikola et al., 2015). Briefly, after ~5h of non-shivering cold exposure, participants were administered a 185 MBq bolus of 2-deoxy-2-[^{18}F]fluoroglucose (^{18}FDG). Approximately 60 min later, a PET-CT scan (General Electric Medical Systems, Milwaukee, WI, USA) was performed in order to visualize supraclavicular ^{18}FDG uptake. BAT volume (mls) and activity (total glucose uptake) were calculated as described previously (Chondronikola et al., 2015; Chondronikola et al., 2014). After the location of ^{18}FDG uptake was identified on participants, the skin was sterilized prior to the injection of 2-5 ml of 2% lidocaine for local anesthesia. A small incision was then made in the skin (~1 cm) so that a 5 mm suction adapted Bergström needle (Stille, Lombard, IL, USA) could be advanced into the sBAT depot for sampling. Immediately after sBAT was sampled, subcutaneous white adipose tissue was sampled from the abdomen (~2 cm from the umbilicus) using a 5 mm suction adapted Bergström needle.

Skeletal muscle sampling

Skeletal muscle biopsies were collected from the mid-point of the *m. vastus lateralis* of young healthy men (n=6) under local lidocaine anesthesia using a suction adapted 5 mm Bergström needle(Bergström, 1975) (Stille, Lombard, IL, USA).

Mouse experiments

All animal procedures were performed in-line with guidelines set forward by the National Institutes of Health regarding the use of animals in research experiments. All animal experiments described here were reviewed and approved by the Institutional Animal Care and Use Committee at the University of Texas Medical Branch. Young (8-12 weeks old) male balb-c mice were used. All animals were housed in a 12:12 light-cycle with free access to rodent chow and water. In line with the Guide for the Care and Use of Laboratory Animals, which recommends for housing laboratory rodents at 20-26°C, temperature were maintained within the animal vivarium between 21.5-22.5°C.

Tissue Sample Handling

All adipose and muscle samples collected from human subjects and animals were rinsed in phosphate buffered saline immediately upon collection. A portion of tissue was immediately submerged in an ice-cold biopsy preservation buffer (pH 7.1) containing 10 mM CaK_2-EGTA; 7.23 mM K_2-EGTA; 20 mM imidazole; 20 mM taurine 50 mM K-MES; 0.5 mM dithiothreitol; 6.56 $MgCl_2$; 5.77 mM ATP and 15 mM creatine phosphate (pH of 7.1). Samples were kept in this ice-cold buffer and immediately transferred to the

laboratory for high-resolution respirometry (HRR) experiments. The amount of tissue used for HRR experiments ranged from 5-10 mg for skeletal muscle and sBAT/iBAT and from 10-20 mg and 50-100 mg for iWAT and sWAT, respectively. A second portion of adipose tissue from each participant/animal was snap frozen in liquid nitrogen and stored at -80°C for gene analyses. In addition, when available, adipose tissue was also preserved in 10% phosphate buffered formalin and 2.5% glutaraldehyde for histology and electron microscopy.

Light, fluorescence and electron microscopy

For light microscopy, adipose tissue samples were dehydrated and paraffin embedded prior to sectioning. 5 µM sections were then stained with hematoxylin and eosin and images captured using an Olympus BX41 light microscope (Olympus Corporation, NJ). For electron microscopy, adipose tissue samples were fixed in 2.5% glutaraldehyde in sodium cacodylate buffer (Electron Microscopy Sciences, Hatfield, PA), followed by 1% osmium tetroxide. Adipose tissue samples were then embedded in an Epon-Araldite mixture and ultra-thin (80 nm) sections were obtained with an Ultracut E ultra-microtome (Leica Microsystems, Buffalo Grove, IL). Ultra-thin sections were examined and images captured with a JEOL 100CX transmission electron microscope (JEOL USA, Inc., MA). For fluorescence microscopy, immunolocalization of antigens was performed in paraffin sections of formalin-fixed tissues as described (Daquinag et al., 2015; Daquinag et al., 2011) upon EDTA-based antigen retrieval, washing with 0.3% Triton X-100 and blocking in Serum-Free Protein Block (DAKO). Primary antibodies (4^{o}C, 12-16 hr) and secondary

antibodies (RT, 1 hr) were applied in PBS / 0.05% Tween-20. The following primary antibodies were used: Rabbit anti-perilipin D418 (Cell Signaling, 1:100), rabbit anti-caveolin-1 D46G3 (Cell Signaling, 1:100) and goat anti-UCP1 (GeneTex, 1:75). Secondary IgG used: donkey Alexa488-conjugated (Invitrogen) and Cy3-conjugated (Jackson). Nuclei were stained with TOPRO3 (Invitrogen). Confocal images were acquired at 20X with TCS SP5 / LAS AF software (Leica).

High Resolution Respirometery

All respiration measurements were performed on one of four Oroboros O2K respirometers (Oroboros Instruments, Innsbruck, Austria). Each day, background calibrations were performed on each polygraphic oxygen sensor (POS) in respiration buffer at air saturation. Zero oxygen and instrumental background calibrations were performed at regular intervals (approximately monthly) during data collection using dithionite titrations. These steps were taken to insure acceptable instrumental background (±1 pmol/s/ml) and stability over time. This is an important consideration in prospective human and animals studies, were quantitative data is required for comparisons of samples collected over time.

All HRR measurements were performed in a respiration buffer (pH 7.1) containing 0.5 mM EGTA; 3 mM $MgCl_2$; 60 mM K-lactobionate; 20 mM taurine; 10 mM KH_2PO_4; 20 mM HEPES; 110 mM sucrose; and 1 mg/ml essential fatty acid free bovine serum albumin. Temperature was maintained at 37±0.01°C during all HRR assays. O_2 concentration within the respiration buffer was recorded at 2-4 s intervals, from which mass specific O_2 fluxes (VO_2 per mg of tissue) were calculated in the pico-molar range

(DatLab, Oroboros Instruments, Innsbruck, Austria). O_2 concentration was maintained between 200-400 µM in the respiration buffer, which was stirred rigorously by a magnetic stir bar to minimize any oxygen dependency artifacts from the data.

All HRR measurements were made on the same day as sample collection. Typically, sample preparation began as soon as possible after biopsy collection of animal sacrifice (<60 min). First, tissue samples were dissected under low magnification to remove any visible blood or connective tissue. Adipose tissue samples were cut into small pieces (5-10 mg each) using sharp scissors or a scalpel. For skeletal muscle biopsies, myofibers were gently separated into ~1 mg bundles using fine forceps. All sample preparation was performed while tissue was bathed in ice-cold biopsy preservation buffer. In order to fully permeabilize the plasma membrane of skeletal muscle samples, myofiber bundles were agitated in biopsy preservation buffer containing 5 µM saponin for ~20 min at 4°C.

Tissue samples were blotted briefly on filter paper, then weighed on a precision micro-balance (Mettler-Toledo, Belgium). Tissue samples were then transferred into the chamber of an O2K for HRR analysis. For sWAT, iWAT, sBAT and iBAT, 2µM digitonin was titrated into the O2K chamber to permeabilize the plasma membrane(Kraunsøe et al., 2010). In order to comprehensively interrogate mitochondrial respiratory capacity, coupling control, and UCP1 function, three different substrate, inhibitor, uncoupler titrations (SUIT) protocols were employed.

In order to directly assay UCP1 dependent respiration, a SUIT protocol was devised where saturating levels of the substrates octanoyl-l-carnitine (1.5 mM), pyruvate (5 mM),

malate (2 mM), glutamate (10 mM) and succinate (10 mM) were titrated into the O2K chamber in order to support leak (state 2) respiration with parallel electron transfer through complex I and II of the electron transfer chain, the electron transferring flavoprotein, and glycerol-3-phosphate dehydrogenase. Then, 20 mM of the UCP1 inhibitor guanosine diphosphate (GDP) (Matthias et al., 1999; Nedergaard et al., 2001; Shabalina et al., 2013) was titrated into the O2K chamber. This approach allowed UCP1 dependent respiration (i.e., UCP1 function) to be assayed directly (Porter et al., 2015).

We also assayed mitochondrial coupling control in a separate SUIT protocol by titration of saturating levels of the substrates octanoyl-l-carnitine (1.5 mM), pyruvate (5 mM), malate (2 mM), glutamate (10 mM), followed by the titration of 5 mM ADP to coupled respiration to ATP production. Then, succinate (10 mM) was titrated into the oxygraph chamber to assay maximal coupled respiration, and finally maximal leak respiration (state 4_O respiration) was determined after titration of the ATP synthase inhibitor oligomycin (5 µM).

Finally, we also assayed mitochondrial flux control in a third SUIT protocol. Saturating levels of the substrates octanoyl-l-carnitine (1.5 mM), pyruvate (5 mM), malate (2 mM), and glutamate (10 mM) where titrated into the O2K chamber to determine leak respiration. Then, 5 mM ADP was titrated to couple respiration to ATP production. Succinate (10 mM) was titrated into the O2K chamber to assay maximal coupled respiration. Thereafter, cytochrome C (10 µM) was titrated to ensure that the mitochondrial outer membranes were intact. Mitochondrial respiratory capacity was determined after titration of proton ionophore carbonyl cyanide *m*-chlorophenyl hydrazone (CCCP) to a final concentration of 5 µM.

Citrate synthase activity

Citrate synthase (CS) activity was measured as a surrogate of mitochondrial protein abundance (Larsen et al., 2012). Tissue homogenates (5 mg/ml for BAT and 50 mg/ml for WAT) were prepared in 175 mM KCl solution containing 2 mM EDTA and 1% Triton. Following homogenization (30-60 s in a glass tissue grinder), samples were snap-frozen and thawed twice to ensure lysing of cells and membranes. Homogenates were centrifuged (3500 × g for 2 min at 4°C), and supernatants recovered for analysis. CS activity was determined in diluted extracts in a 100 mM phosphate buffer (pH 7.1) containing 10 mM 5,5'-dithiobis-(2-nitrobenzoic acid) (DTNB) and 30 mM acetyl-CoA (Srere, 1969). After the addition of 10 mM oxaloacetate, free coenzyme A produced from the condensation of acetyl-CoA and oxaloacetate was bound to DTNB, and resulting change in light absorbance, detected spectrophotometrically at 412 nm Eon™ (BioTek Instruments, Winooski, VT, USA), was used to determine the activity of citrate synthase (nmol/g/s).

Cytochrome C oxidase activity.

Cytochrome C oxidase (COX) activity was measured in the same adipose tissue lysates prepared for CS activity. Maximal COX activity was determined in and Oroboros O2K respirometer (Oroboros Instruments, Innsbruck, Austria). Assays were performed in the same respiration buffer as detailed above with some minor modifications. To block electron transfer proximal to COX, 2.5µm Antimyin A was added to the respiration

buffer. Maximal respiration was then assayed following the titration of the electron donor *N,N,N′*,*N′*-tetramethyl-1,4-benzenediamine dihydrochloride (TMPD, 500μm) in the presence of ascorbate (2mM) and reduced cytochrome C (10μm). Blanks were also ran in the presense of TMPD, ascorbate and cytochrome C do account for auto-oxidation. The peak in respiration for samples and blanks was used to calculate COX activity, expressed as O_2 flux (nmol/s/mg).

Gene expression

Approximately 50-100 mg of adipose was used for extraction of RNA using a pure link RNA isolation mini kit (Life Technologies, Carlsbad, CA). cDNA was synthesized and amplified using a high capacity RNA-cDNA kit and TaqMan pre Amp master mix kit, respectively (Life Technologies, Carlsbad, CA). Quantitative real-time PCR analyses were performed on an ABI PRISM 7900HT using standard TaqMan master-mix reagents and gene-specific primer assays (Life Technologies, Carlsbad, CA). GAPDH was used as the housekeeping gene to normalize the expression of the target gene.

REFERENCES

Bergström, J. (1975). Percutaneous needle biopsy of skeletal muscle in physiological and clinical research. Scand J Clin Lab Invest *35*, 609–616.

Chondronikola, M., Annamalai, P., Chao, T., Porter, C., Saraf, M., Cesani, F., and Sidossis, L. (2015). A percutaneous needle biopsy technique for sampling the supraclavicular brown adipose tissue depot of humans. Int J Obes (Lond), Epub ahead of print.

Chondronikola, M., Volpi, E., Børsheim, E., Porter, C., Annamalai, P., Enerbäk, S., Liddell ME, Saraf, M., Labbe, S., Hurren, S*., et al.* (2014). Brown adipose tissue activation improves glucose homeostasis and insulin sensitivity in humans. Diabetes *63*, 4089-4099.

Daquinag, A., Tseng, C., Salameh, A., Zhang, Y., Amaya-Manzanares, F., Dadbin, A., Florez, F., Xu, Y., Tong, Q., and Kolonin, M. (2015). Depletion of white adipocyte progenitors induces beige adipocyte differentiation and suppresses obesity development. Cell Death Differ *22*, 351-363.

Daquinag, A., Zhang, Y., Amaya-Manzanares, F., Simmons, P., and Kolonin, M. (2011). An isoform of decorin is a resistin receptor on the surface of adipose progenitor cells Cell Stem Cell *9*, 74-86.

Kraunsøe, R., Boushel, R., Hansen, C., Schjerling, P., Qvortrup, K., Støckel, M., Mikines, K., and Dela, F. (2010). Mitochondrial respiration in subcutaneous and visceral adipose tissue from patients with morbid obesity. J Physiol *588*, 2023-2032.

Larsen, S., Nielsen, J., Hansen, C.N., Nielsen, L.B., Wibrand, F., Stride, N., Schroder, H.D., Boushel, R., Helge, J.W., Dela, F.*, et al.* (2012). Biomarkers of mitochondrial content in skeletal muscle of healthy young human subjects. J Physiol *590*, 3349-3360.

Matthias, A., Jacobsson, A., Cannon, B., and Nedergaard, J. (1999). The bioenergetics of brown fat mitochondria from UCP1-ablated mice. Ucp1 is not involved in fatty acid-induced de-energization ("uncoupling"). J Biol Chem *274*, 28150-28160.

Nedergaard, J., Golozoubova, V., Matthias, A., Asadi, A., Jacobsson, A., and Cannon, B. (2001). UCP1: the only protein able to mediate adaptive non-shivering thermogenesis and metabolic inefficiency. Biochim Biophys Acta *1504*, 82-106.

Porter, C., Herndon, D., Bhattarai, N., Ogunbileje, J., Szczesny, B., Szabo, C., Toliver-Kinsky, T., and Sidossis, L. (2015). Severe Burn Injury Induces Thermogenically Functional Mitochondria in Murine White Adipose Tissue. Shock *44*, 258-264.

Shabalina, I., Petrovic, N., de Jong, J., Kalinovich, A., Cannon, B., and Nedergaard, J. (2013). UCP1 in Brite/Beige Adipose Tissue Mitochondria Is Functionally Thermogenic. Cell Rep *5*, 1196-1203.

Srere, P. (1969). Citrate Synthase. Methods Enzymol *13*, 3-11.